



Influence of pH on the Hydrothermal Synthesis of Al-Substituted Smectites (Saponite, Beidellite, and Nontronite)

I. Criouet · J. C. Viennet · F. Baron · E. Balan · A. Buch · L. Delbes · M. Guillaumet · L. Remusat · S. Bernard

Accepted: 1 September 2023 / Published online: 11 October 2023
© The Author(s), under exclusive licence to The Clay Minerals Society 2023

Abstract Smectitic clay minerals are unique indicators of paleoenvironmental conditions and exhibit a unique reactivity in the mineral world. Smectites may exhibit tetrahedral substitutions (Al^{3+} , and sometimes Fe^{3+} , can substitute for Si^{4+} in tetrahedral sites), resulting in a layer-charge increase, thereby impacting their properties (e.g. swelling and sorption capacities, catalytic properties, expandable abilities).

The objective of the present study was to determine the influence of pH conditions on the hydrothermal production of smectite end-members exhibiting tetrahedral Al substitutions (saponite, beidellite, and nontronite), using X-ray diffraction (XRD) and Fourier-transform infrared (FTIR) methods. The results of a series of syntheses conducted at various pH values allowed discussion of the crystallization pathways of these smectites from a mechanistic point of view. Altogether, the present study provided easily reproducible protocols for the hydrothermal production of pure saponite, nontronite, or beidellite (i.e. with no other mineral). The successful synthesis of pure saponite was achieved by exposing the starting gels to 230°C for 4 days in solutions at pH ranging from 5.5 to 14. The successful synthesis of pure beidellite was achieved by exposing the starting gels to 230°C for 9 days in a solution at pH 12. The successful synthesis of pure nontronite was achieved by exposing the starting gels to 150°C for 2.5 days in a solution at pH 12.5. Although extrapolating experimental results to natural settings remains difficult, the results of the present study may be of great help to constrain better the geochemical conditions existing or having existed on extraterrestrial planetary bodies.

Associate Editor: F. Javier Huertas

Supplementary Information The online version contains supplementary material available at <https://doi.org/10.1007/s42860-023-00255-3>.

I. Criouet · J. C. Viennet · E. Balan · L. Delbes · M. Guillaumet · L. Remusat · S. Bernard (✉)
Institut de Minéralogie, de Physique des Matériaux et de Cosmochimie (IMPMC), Muséum National d'Histoire Naturelle, Sorbonne Université, CNRS UMR 7590, Paris, France
e-mail: sbernard@mnhn.fr

J. C. Viennet
Unité Matériaux et Transformations (UMET), Université de Lille, INRA, ENSCL, CNRS UMR 8207, Lille, France

F. Baron
Institut de Chimie des Milieux et Matériaux de Poitiers (IC2MP), Université de Poitiers, CNRS UMR 7285, Poitiers, France

A. Buch
Laboratoire Génie des Procédés et Matériaux (LGPM), CentraleSupélec, Gif-Sur-Yvette, France

Keywords Smectite · pH · Hydrothermal synthesis · XRD · FTIR

Introduction

Smectitic clay minerals are widespread in the Solar System (Hazen et al., 2013) and can form in many contexts, from alteration settings to magmatic systems, in wide ranges of redox and pH conditions (Fox et al., 2021; Meunier, 2005; Meunier et al., 2008; Viennet et al., 2017, 2020, 2021; Zhou & Keeling, 2013). These strongly anisotropic minerals carry key information about the geochemistry, oxidation state, and water content of the environments in which they were produced (Ehlmann et al., 2011; Fox et al., 2021), making them good indicators of paleoenvironmental and paleoclimatic conditions. Their intrinsic properties (e.g. adsorption capacity, catalytic properties) confer on them a unique reactivity in the mineral world, explaining their huge number of applications in a variety of domains (e.g. Carniato et al., 2020; Choy et al., 2007; Murray, 1991, 2000), including medicine (Ghadiri et al., 2015; Saadat et al., 2022), pharmaceuticals (Bello et al., 2022; Carretero & Pozo, 2009; Corbin et al., 2021), pollution control (Churchman et al., 2006; Ewis et al., 2022), the petroleum industry (Abdo & Haneef, 2013; Li et al., 2023; Salter et al., 2023), and the construction industry (Singh, 2022). It is the exceptional trapping capabilities of smectites that make possible the geological storage of CO₂ or H₂ (Abdullelah et al., 2023; de Jong et al., 2014; Ho et al., 2023; Romanov, 2013; Rother et al., 2013) and radioactive waste (Delage et al., 2010; Landais et al., 2013; Parrotin et al., 2023; Robin et al., 2017). Smectite-rich rocks are also a major reservoir of Rare Earth Elements (Abbott et al., 2019; Moldoveanu & Papangelakis, 2012), and the strong affinities of smectites for organic molecules make them the primary agents for organic carbon sequestration in soils, sediments, and chondrites (Blattmann et al., 2019; Kennedy et al., 2002; Viennet et al., 2023) and the probable main actors of the origins of life (Kloprogge & Hartman, 2022; Viennet et al., 2021). Because they are also the main carriers of water in sediments and in the oceanic crust, smectitic rocks play a great role in subduction settings (Hwang et al., 2017; Katayama et al., 2015). Their anisotropic nature affects the seismic properties of rocks (Almqvist & Mainprice, 2017), as well as the macroscopic behavior of faults (Ikari et al., 2009).

Smectites are clay minerals with a 2:1 layer silicate structure, each layer being made of an octahedral sheet sandwiched between two Si(Al,Fe³⁺)–O

tetrahedral sheets and in which stacking creates expandable interlayer spaces capable of storing water, organics, and exchangeable cations (mostly Ca²⁺, Mg²⁺, Na⁺, and K⁺) balancing the overall charge (Fox et al., 2021; Meunier, 2005). While trioctahedral smectites (such as hectorite and saponite) have all octahedral sites filled by mostly divalent cations, dioctahedral smectites (such as nontronite, montmorillonite, and beidellite) have only two of their three octahedral sites filled by mostly trivalent cations, the most common octahedral cations being Al, Fe, and Mg. Depending on the pH conditions under which they crystallize, smectites may exhibit tetrahedral substitutions (Al³⁺, and sometimes Fe³⁺, can substitute for Si⁴⁺ in tetrahedral sites), resulting in an increase in layer charge, thereby impacting their properties, such as their swelling or sorption capacities, catalytic properties, or expansion abilities (Fox et al., 2021; Komadel et al., 2005; Meunier, 2005; Murray, 2000).

Many studies dealing with the synthesis of smectites exist in the literature (Dzene et al., 2018; Kloprogge, 1999; Petit et al., 2017; Ponce & Kloprogge, 2020; Zhang et al., 2010). Although smectites could be synthesized from glasses submitted to high-pressure and high-temperature conditions (Kalo et al., 2010; Nakazawa et al., 1992; Tamura, 2000; Yamada, 1994, 1995), most syntheses are conducted following the sol-gel method, i.e. using gels produced at room temperature before being exposed to hydrothermal conditions. A number of syntheses aimed at producing a suite of smectite samples spanning compositional ranges between Fe(II), Fe(III), Mg, and Al end-member species to document precisely their spectroscopic signatures, was carried out recently by Fox et al. (2021). In parallel, a number of laboratory studies have investigated how conditions (such as temperature and pH) control cation coordination and incorporation into the smectite structure and, in turn, their final crystallochemistry (Andrieux & Petit, 2010; Baron et al., 2016a, b; Blukis et al., 2022; Grauby et al., 1993, 1994; Harder, 1976; Huertas et al., 2000; Petit et al., 2015, 2017). For instance, Blukis et al. (2022) recently showed that high pH favors a high degree of crystallinity for saponite. However, those studies were dedicated to a given end-member or to a given solid solution (i.e. either the Fe(III)–Mg (nontronite–saponite) or the Fe(III)–Al (nontronite–beidellite) series (Andrieux & Petit, 2010; Grauby et al., 1993, 1994; Petit et al., 2015)).

Because the speciation of Fe, Mg, and Al as a function of pH is different (Millero et al., 1995; Perry & Shafran, 2001; See et al., 2015; Pierrot & Millero, 2017; de Mello Gabriel et al., 2021), the optimal pH for the synthesis of saponite, beidellite, and nontronite is anticipated to be different, with pH conditions strongly influencing their production. The sensitivity of different smectites to pH conditions thus remains to be investigated. The purpose of the present study, therefore, was to investigate the influence of pH conditions on the production of smectites, using three different series of hydrothermal syntheses designed to lead (when conditions are optimal) to the crystallization of three smectite end-members containing tetrahedral Al, namely a saponite ($\text{Na}_{0.4}(\text{Si}_{3.6}\text{Al}_{0.4})\text{Mg}_3\text{O}_{10}(\text{OH})_2$), a beidellite ($\text{Na}_{0.4}(\text{Si}_{3.6}\text{Al}_{0.4})\text{Al}_2\text{O}_{10}(\text{OH})_2$), and a nontronite ($\text{Na}_{0.4}(\text{Si}_{3.6}\text{Al}_{0.4})\text{Fe}^{3+}_2\text{O}_{10}(\text{OH})_2$).

Experimental

Sample Preparation

The syntheses reported here were conducted via a sol–gel method, i.e. using gels produced at room temperature before being exposed to hydrothermal conditions. To explore the influence of pH conditions, the syntheses reported here used gels produced from solutions at various pH and exposed to hydrothermal conditions within solutions at various pH. The preparation of the gels was done following classic protocols (Baron et al., 2016a; Dzene et al., 2018; Fox et al., 2021; Petit et al., 2017). Starting solutions were mixed to obtain gels with the Si:Al:Mg, Si:Al:Al, and Si:Al:Fe molar ratios of pure Al-substituted smectite end-members (i.e. 3.6:0.4:3 for the saponite, 3.6:0.4:2 for the beidellite, and 3.6:0.4:2 for the nontronite). For all gels, the first step was to pour an AlCl_3 solution into a Na_2SiO_3 solution under continuous stirring at room temperature, which led to the instantaneous formation of a white precipitate of amorphous aluminosilicate. Then, a given volume of either a MgCl_2 , an FeCl_3 , or an AlCl_3 solution was added to provide the exact quantity of cations needed for the octahedral occupancies. Stirring was stopped soon after this step, and the precipitated gel was filtered and rinsed with pure water with a vacuum suction filter device to remove excess salts. Each starting gel was immersed

in a solution at a given pH in Teflon acid-digestion bombs which were sealed and placed in an oven for several days (syntheses were conducted in pure water or in solutions at pH values ranging from 12 to 14 for saponites and from 12 to 13 for nontronites and beidellites given the high pH sensitivity of these smectites). The synthesized products were then filtered and rinsed with pure water (resistivity of $18.2 \text{ M}\Omega\text{-cm}$) to remove any remaining salt. Then, they were dried in an oven at 50°C for 24 h and ground in an agate mortar for characterization using X-ray diffraction (XRD) and Fourier-transform infrared spectroscopy (FTIR) as classically done for smectites (Baron et al., 2016a; Dzene et al., 2018; Fox et al., 2021; Petit et al., 2017).

Measurements and Characterization

The pH of each starting solution, i.e. the solution in equilibrium with the gel and the solution in equilibrium with the products of syntheses, was measured using a Fisher Scientific (Hampton, New Hampshire, USA) Accumet XL600 pH/mV/Temp/ISE/DO/Conductivity Meter calibrated with three buffers (pH 7, 10, and 12). The uncertainty for each measurement was estimated to be ± 0.05 pH units. The *PhreeqC* code associated with the *minteq.v4* database was used to determine the major species in the starting solutions used for the production of gels.

The XRD data reported here were collected on unoriented powders at room temperature with a step size of $0.033^\circ 2\theta$ over the $4\text{--}75^\circ 2\theta$ $\text{CoK}\alpha_{1,2}$ (40 mA, 45 kV) angular range and a counting time of 300 ms per step using an X'Pert Pro instrument from Malvern PANalytical (Malvern, UK), operating at the Institut de Minéralogie, de Physique des Matériaux et de Cosmochimie (IMPMC, Paris, France).

The FTIR data shown here were collected on unoriented powders in attenuated total reflection mode (ATR) with a diamond internal reflexion element with a 4 cm^{-1} resolution in the mid-infrared (MIR) range ($4000\text{--}400 \text{ cm}^{-1}$) using a Fisher Scientific (Hampton, New Hampshire, USA) Nicolet 6700 FTIR spectrometer equipped with a KBr beamsplitter and DTGS-KBr detector and operating at the Institut de Minéralogie, de Physique des Matériaux et de Cosmochimie (IMPMC, Paris, France).

Starting Solutions

Dilute solutions (0.2 M) of Na_2SiO_3 (>95%), AlCl_3 (99%), MgCl_2 (>99%), and FeCl_3 (>99%) were prepared using pure water (milliQ—18.2 M Ω -cm) for the syntheses reported here, leading to a Na_2SiO_3 solution at pH 13.1, a MgCl_2 solution at pH 5.4, an FeCl_3 solution at pH 1.8, and an AlCl_3 solution at pH 3.4 (Table 1). Some NaOH was added to the AlCl_3 and FeCl_3 solutions to obtain an additional FeCl_3 solution at pH 2.1 and four additional AlCl_3 solutions at pH 3.9, 5.3, 8.0, and 10.6 (Table 1). These additional solutions were used to test the influence of the pH of the starting solutions on the synthesis of nontronite and beidellite. All chemicals were obtained from Sigma Aldrich (St. Louis, Missouri, USA)..

Detailed Protocols

Saponite syntheses

Four different syntheses were conducted from the gel of saponite composition for the present study. The starting gels were prepared by pouring 556 μL of the AlCl_3 solution at pH 3.4 into 5 mL of the Na_2SiO_3 solution, before being mixed with 4.17 mL of the MgCl_2 solution, to produce, theoretically, ~100 mg of a gel stoichiometrically identical to a pure saponite with 0.4 Al in each tetrahedron ($\text{Na}_{0.4}(\text{Si}_{3.6}\text{Al}_{0.4})\text{Mg}_3\text{O}_{10}(\text{OH})_2$). The pH of the solution in equilibrium with the gel was ~10. After filtration, the gel produced was placed into 23 mL Teflon reactors before

drying and immersed in 16.5 mL of pure water at pH 5.5 (i.e. pure water in equilibrium with atmospheric CO_2) or in 16.5 mL of a solution composed of pure water in which was added NaOH to reach a pH of 12, 13, or 14 (cf Table 2). All reactors were then put in an oven at 230°C (~28 bar) for 4 days, following the recommendations of Zhang et al. (2020) for the synthesis of pure saponites. During syntheses above 200°C, saponite particles grow faster during the first 3 days than during the subsequent 10 (Zhang et al., 2020). Of note, although saponites can be produced at low temperature (i.e. 90°C; Meyer et al., 2020; Ponce & Klopogge, 2020), high temperature conditions inhibit the incorporation of Al into octahedral sheets, while enhancing $^{[4]}\text{Al}^{3+}$ for $^{[4]}\text{Si}^{4+}$ tetrahedral substitutions, as reported by Klopogge and Ponce (2021).

Beidellite Syntheses

Four different syntheses were conducted from the gel of beidellite composition for the present study. The starting gels were prepared by pouring 2.833 mL of the AlCl_3 solution at pH 3.9 into 4.25 mL of the Na_2SiO_3 solution to produce theoretically ~80 mg of a gel stoichiometrically identical to a pure beidellite with 0.4 Al in each tetrahedron ($\text{Na}_{0.4}(\text{Si}_{3.6}\text{Al}_{0.4})\text{Al}_2\text{O}_{10}(\text{OH})_2$). The pH of the solution at room temperature in equilibrium with the gel was ~4.5. After filtration, the produced gel was kept hydrated and placed into 23 mL Teflon reactors and immersed into 12.5 mL of pure water at pH 5.5 (i.e. pure water in equilibrium with atmospheric CO_2) or into 12.5 mL

Table 1 pH of the starting solutions (0.2 mol.L⁻¹) and the main Si, Al, Fe, and Mg species in solution at 20°C (calculated using *PhreeqC*)

Solutions	pH	Major species in solution	Color of the solution
Na_2SiO_3 (0.2 M)	13.1	$\text{H}_2\text{SiO}_4^{2-}/\text{H}_3\text{SiO}_4^-$	Transparent
AlCl_3 (0.2 M)	3.4	Al^{3+}	Transparent
FeCl_3 (0.2 M)	1.8	Fe^{3+}	Yellow
MgCl_2 (0.2 M)	5.4	Mg^{2+}	Transparent
FeCl_3 (0.2 M) + NaOH	2.1	$\text{Fe}^{3+} > \text{Fe}_2(\text{OH})_2^{4+} > \text{FeCl}^{2+} > \text{FeOH}^{2+}$	Orange
AlCl_3 (0.2 M) + NaOH	3.9	$\text{Al}^{3+} > > > \text{Al}(\text{OH})^{2+}$	Transparent
AlCl_3 (0.2 M) + NaOH	5.3	$\text{Al}^{3+} > \text{Al}(\text{OH})^{2+} > \text{Al}(\text{OH})_2^+$	White (+ solid $\text{Al}(\text{OH})_3$)
AlCl_3 (0.2 M) + NaOH	8	$\text{Al}(\text{OH})_4^-$	White (+ solid $\text{Al}(\text{OH})_3$)
AlCl_3 (0.2 M) + NaOH	10.6	$\text{Al}(\text{OH})_4^-$	White (+ solid $\text{Al}(\text{OH})_3$)

Table 2 Details of the syntheses

Expected product	pH of the Na ₂ SiO ₃ solution	pH of the AlCl ₃ solution	pH of the third solution	Theoretical mass of gel (mg)	pH of the solution in equilibrium with the gel	Volume of the added solution (mL)	pH of the added solution	Temperature (°C)	Duration (days)	pH of the solution in equilibrium with the final products	Final products
Saponite	13.1	3.4	5.4 (MgCl ₂)	100	10	16.5	5.5	230	4	7.5	Saponite
Saponite	13.1	3.4	5.4 (MgCl ₂)	100	10	16.5	12	230	4	10.4	Saponite
Saponite	13.1	3.4	5.4 (MgCl ₂)	100	10	16.5	13	230	4	12.9	Saponite
Saponite	13.1	3.4	5.4 (MgCl ₂)	100	10	16.5	14	230	4	13.7	Saponite
Beidellite	13.1	3.9	3.9 (AlCl ₃)	80	4.5	12.5	5.5	230	9	7.2	Kaolins
Beidellite	13.1	3.9	3.9 (AlCl ₃)	80	4.5	12.5	12	230	9	9.4	Beidellite
Beidellite	13.1	3.9	3.9 (AlCl ₃)	80	4.5	12.5	12.5	230	9	11	Beidellite + Analcime
Beidellite	13.1	3.9	3.9 (AlCl ₃)	80	4.5	12.5	13	230	9	12	Analcime
Nontronite	13.1	3.4	2.1 (FeCl ₃)	165	4	16.5	5.5	150	2.5	4.7	Hisingerite
Nontronite	13.1	3.4	2.1 (FeCl ₃)	165	4	16.5	12	150	2.5	8.3	Amorphous Gel
Nontronite	13.1	3.4	2.1 (FeCl ₃)	165	4	16.5	12.5	150	2.5	10.7	[⁴]Fe-Nontronite
Nontronite	13.1	3.4	2.1 (FeCl ₃)	165	4	16.5	13	150	2.5	12.7	[⁴]Fe-Nontronite + Analcime
Nontronite	13.1	5.3	2.1 (FeCl ₃)	165	–	16.5	12.5	150	2.5	–	[⁴]Fe-Nontronite + Hisingerite
Nontronite	13.1	8.0	2.1 (FeCl ₃)	165	–	16.5	12.5	150	2.5	–	[⁴]Fe-Nontronite
Nontronite	13.1	10.6	2.1 (FeCl ₃)	165	9	16.5	5.5	150	2.5	9.7	[⁴]Fe-Nontronite + Bay-erite
Nontronite	13.1	10.6	2.1 (FeCl ₃)	165	9	16.5	12	150	2.5	12.1	[⁴]Fe-Nontronite + Bay-erite
Nontronite	13.1	10.6	2.1 (FeCl ₃)	165	9	16.5	12.5	150	2.5	12.5	[⁴]Al-Nontronite
Nontronite	13.1	10.6	2.1 (FeCl ₃)	165	9	16.5	13	150	2.5	12.9	[⁴]Fe-Nontronite

of a solution composed of pure water to which was added NaOH to reach a pH of 12, 12.5, or 13 (cf Table 2). Only 12.5 mL of pure water or solution at pH 12, 12.5, or 13 was used rather than 16.5 mL to prevent overpressure related to the swelling of the gel containing a lot of highly hydrated Al^{3+} . All reactors were then placed in an oven at 230°C (~28 bar) for 9 days, previous successful syntheses having been conducted over 8 to 10 days from 175–200°C (De Kimpe, 1976; Klopogge et al., 1993) to well above 300°C (Klopogge et al., 1990; Lantenois et al., 2008).

Nontronite Syntheses

Three different series of syntheses were conducted from four different gels of nontronite composition for the present study. A first series of four syntheses was conducted with a gel produced using the AlCl_3 solution at pH 3.4, a second series of four syntheses was conducted with a gel produced using the AlCl_3 solution at pH 10.6, and a third series of two syntheses was conducted with either a gel produced using the AlCl_3 solution at pH 5.3 or a gel produced using the AlCl_3 solution at pH 8. Each starting gel was prepared by pouring 833 μL of the AlCl_3 solution into 7.5 mL of the Na_2SiO_3 solution, before being mixed with 4.17 mL of the FeCl_3 solution, to produce, theoretically, ~165 mg of a gel stoichiometrically identical to a pure nontronite with 0.4 Al in each tetrahedron ($\text{Na}_{0.4}(\text{Si}_{3.6}\text{Al}_{0.4})\text{Fe(III)}_2\text{O}_{10}(\text{OH})_2$). The pH of the solution in equilibrium with the gel prepared with the AlCl_3 solution at pH 3.4 was ~4, while that formed with the AlCl_3 solution at pH 10.6 reached a pH of 9. After filtration, all the gels produced were kept hydrated and placed in 23 mL Teflon reactors. The gels produced using either the AlCl_3 solution at pH 3.4 or the AlCl_3 solution at pH 10.6 were immersed in 16.5 mL of pure water at pH 5.5 (i.e. pure water in equilibrium with atmospheric CO_2) or in 16.5 mL of a solution composed of pure water to which was added NaOH to reach a pH of 12, 12.5, or 13, while the two gels produced using either the AlCl_3 solution at pH 5.3 or the AlCl_3 solution at pH 8 were immersed only in 16.5 mL of a solution composed of pure water to which was added NaOH to reach a pH of 12.5 (cf Table 2). All reactors were then placed in an oven at 150°C (4.75 bar) for 2.5 days, following the recommendations of Andrieux and Petit (2010),

Baron et al. (2016a), and Dzene et al. (2022). In fact, higher temperatures (>200°C) may favor the formation of kaolinite, hematite (akaganeite), or aegirine (Andrieux & Petit, 2010; Decarreau et al., 2008; Delvaux et al., 1989).

Results

Saponite Syntheses

Each of the four syntheses produced a translucent, gelatinous solid residue immersed in a transparent solution at a pH close to that of the solutions in which the starting gels were immersed (i.e. 7.5 for the synthesis conducted in pure water, 10.4 in the solution at pH 12, 12.9 in the solution at pH 13, and 13.7 in the solution at pH 14; cf Table 2). These residues turned white upon drying.

Whatever the pH of the solution used for the syntheses, the XRD patterns of the synthetic products exhibited peaks typical of the *hkl* reflections of 2:1 trioctahedral saponites (Grauby et al., 1994), i.e. peaks at ~12.7 Å (001), 4.55 Å (02,11), ~3.10 Å (004), 2.60 Å (13,20), 1.73 Å (15,24,31), and ~1.53 Å (06,33) (Fig. 1). The 06,33 reflection of these saponites confirmed their trioctahedral nature (>1.51 Å; Brown & Brindley, 1980; Decarreau et al., 1992; Grauby et al., 1994), and the position of the 001 reflections indicated that they were mainly monohydrated (Brown & Brindley, 1980; Ferrage et al., 2005, 2007). Under vacuum, the d_{001} of the saponite synthesized in pure water collapsed to 10.45 Å (Fig. S1). The 02,11 and 06,33 reflections of the saponite synthesized in solution at pH 14 shifted to lower angles compared to saponites synthesized in solutions at lower pH (4.58 to 4.55 Å and 1.533 to 1.526 Å).

All synthetic products had a FTIR spectrum exhibiting a broad band near 3420 cm^{-1} typical of the νOH vibrations of the water adsorbed within the interlayer spaces of smectites (Fig. 2; Madejová et al., 2017). In addition, the FTIR spectra of all synthetic products showed the characteristic bands of saponite, i.e. $\nu\text{Mg}_3\text{OH}$ and $\delta\text{Mg}_3\text{OH}$ vibrations at 3680 and 655 cm^{-1} , respectively; $\nu\text{Si-O}$ vibration near 1000–950 cm^{-1} ; $^{[4]}\text{Al-O}$ out of plane near 800 cm^{-1} ; perpendicular Si-O-Mg vibrations at 692 and 532 cm^{-1} ; and $\delta\text{Si-O-Si}$ vibrations near 500 and 455 cm^{-1} (Klopogge & Ponce, 2021; Madejová

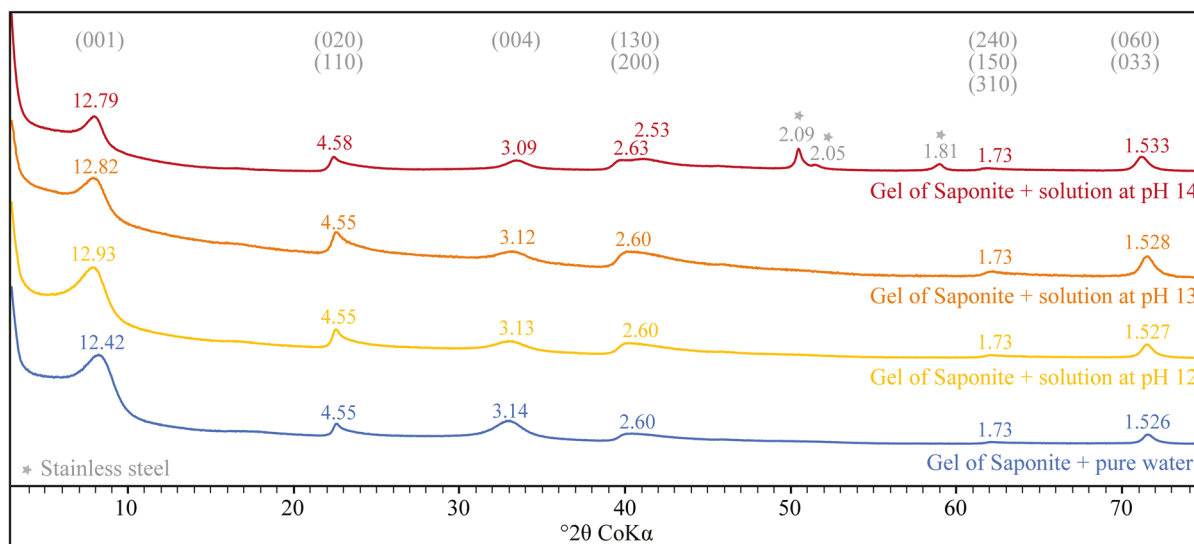


Fig. 1 XRD patterns of products of syntheses conducted with the gels of saponite composition. Peaks at 2.09, 2.05, and 1.80 Å are attributed to contamination by austenitic stainless steel during XRD sample preparation (Boonruang & Sanumang, 2021)

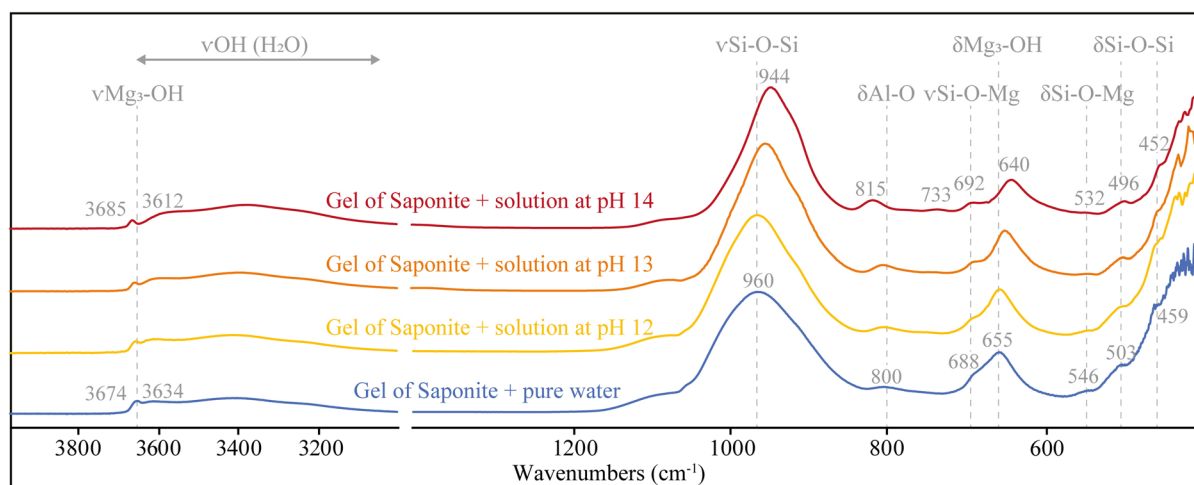


Fig. 2 FTIR spectra of products of syntheses conducted with the gels of saponite composition

et al., 2017). Bands corresponding to $\nu\text{Mg}_3\text{OH}$ and $\delta\text{Mg}_3\text{OH}$ vibrations in the FTIR spectra of the saponite synthesized in solution at pH 14 shifted toward higher and lower wavenumbers compared to FTIR spectra of saponites synthesized in solutions at lower pH. The band near 3612–3634 cm^{-1} is related to the stretching vibration of interlayer water molecules (Fig. S2). In this case, the two OH groups of the molecule are not equivalent and this signal is assigned to

the OH group weakly bonded to the surface oxygens (Farmer, 1974).

Beidellite Syntheses

Each of the four syntheses produced solid residues immersed in a colorless transparent solution at a pH close to that of the solutions in which the starting gels were immersed (i.e. 7.2 for the synthesis conducted in

pure water at pH 5.5, 9.4 in the solution at pH 12, 11 in the solution at pH 12.5, and 12 for the synthesis at pH 13; Table 2).

The synthesis conducted in pure water produced a white and pasty solid residue which became very soft upon drying, showing an XRD pattern typical of kaolins, with peaks at 7.17 Å (001), 4.43 Å (020), 4.34 Å (110), 4.41 Å (111), 3.57 Å (002), 3.39 Å (111), 2.55 Å (201), 2.35 Å (003), 1.79 Å (004), and 1.486 Å (060) (Fig. 3; Carroll, 1970). The bands at 3621 and 3692 cm^{-1} in the FTIR spectrum of this solid confirms the presence of kaolins (Fig. 4; Kodama, 1962; Zhang et al., 2010; Madejová et al., 2017).

The synthesis conducted in the solution at pH 12 produced a translucent, gelatinous solid residue that

turned white, with a paper texture, upon drying. The XRD pattern of this synthetic product revealed the presence of reflections typical of smectitic clay minerals, with peaks at 12.17 Å (001), 6.12 Å (002), 4.43 Å (02,11), 3.09 Å (004), 2.53 Å (13,20), 2.04 Å (006), 1.68 Å (15,24,31), and 1.488 Å (06,33) (Fig. 3). In addition, the basal spacing of the $d(06,33)$ is typical of dioctahedral Al-rich smectites such as beidellite (1.48–1.50 Å Grauby et al., 1994; Petit et al., 2015). Its presence was suggested also by the FTIR spectrum exhibiting characteristic bands of Al-rich smectites, i.e. the bands at 3670 cm^{-1} ($\nu\text{Al}_2\text{OH}$), 3626 cm^{-1} ($\nu\text{Al}_2\text{OH}$), 1000–950 cm^{-1} ($\nu\text{Si-O}$), 914 cm^{-1} ($\delta\text{Al}_2\text{OH}$), 815 cm^{-1} ($^{[4]}\text{Al-O}$ out of plane), 694 cm^{-1} ($^{[6]}\text{Al-O}_{\text{ap}}$), 520 cm^{-1} ($\delta\text{Si-O-}^{[6]}\text{Al}$), and 455 cm^{-1} ($\delta\text{Si-O-Si}$) (Fig. 4; Farmer & Russell,

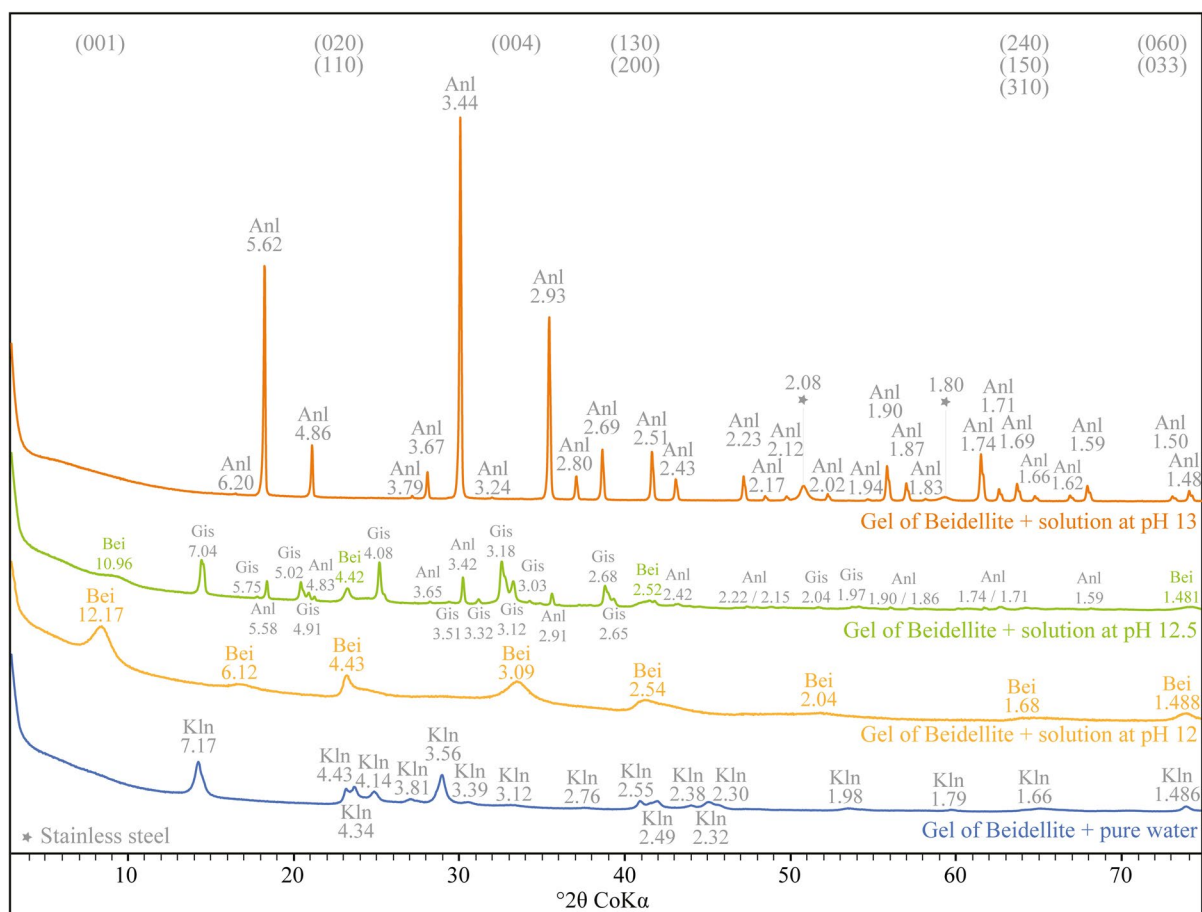


Fig. 3 XRD patterns of products of syntheses conducted with the gels of beidellite composition. Bei: Beidellite. Anl: Analcime. Gis: Gismondine. Kln: Kaolinite. Peaks at 2.08 Å and 1.80 Å are attributed to contamination by austenitic stainless steel during XRD sample preparation (Boonruang & Sanumang, 2021)

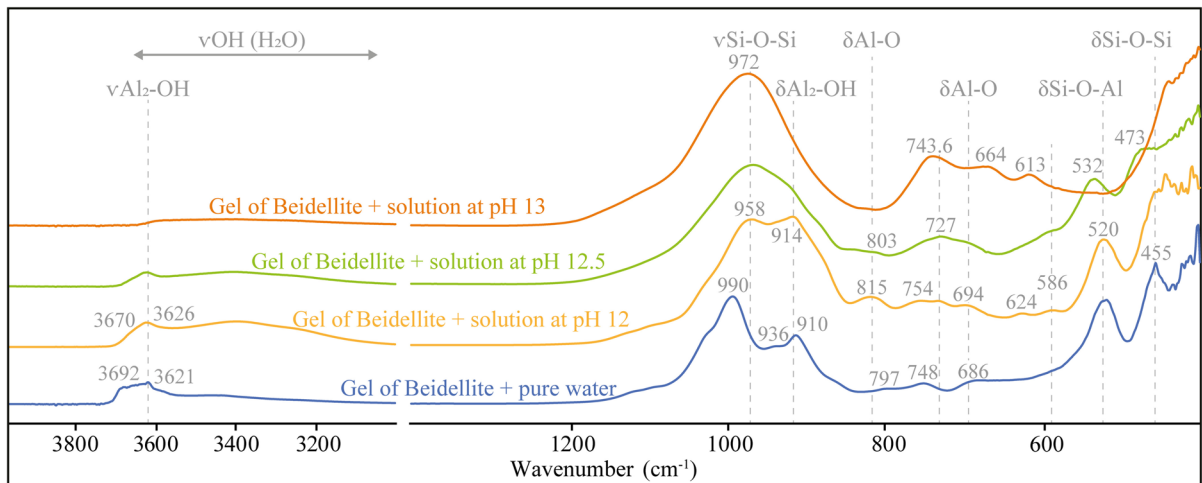


Fig. 4 FTIR spectra of products of syntheses conducted with the gels of beidellite composition

1964; Klopogge et al., 1990; Lantenois et al., 2008; Zviagina et al., 2004). Under vacuum, the d_{001} of the beidellite synthesized in the solution at pH 12 collapsed to 9.78 Å (Fig. S1).

The synthesis conducted in the solution at pH 12.5 produced a solid residue with an XRD pattern exhibiting peaks at 10.96 Å (001), 4.42 Å (02,11), 2.52 Å (13,20), and 1.481 Å (06,33), probably indicating the presence of beidellite (i.e. the $d(06,33)$ diffracts between 1.48 and 1.50 Å; Fig. 3). The weak and broad peak of the (001) reflection indicates its poorly crystalline and dehydrated state (Ferrage et al., 2007). This beidellite cohabits with two zeolites (which are the main phases of the residue): analcime (diffraction peaks at 5.58, 4.83, 3.65, 3.42, 2.91, 2.42, 2.22, 2.15, 1.90, 1.86, 1.74, 1.71, and 1.59 Å) and a Na-garronite-like zeolite (diffraction peaks at 7.04, 5.75, 5.02, 4.91, 4.08, 3.51, 3.32, 3.18, 3.12, 3.03, 2.68, 2.65, 2.04, 1.97, 1.96, and 1.78 Å; Oleksiak et al., 2016; Tayraukham et al., 2020).

The synthesis conducted in the solution at pH 13 produced a grainy solid residue with an XRD pattern typical of analcime, with peaks at 6.20 Å, 5.62 Å (011), 4.86 Å (020), 3.79 Å, 3.67 Å (021), 3.41 Å (222), 3.24 Å, 2.91 Å (112), 2.80 Å (022), 2.69 Å (130), 2.51 Å (231), 2.43 Å (040), 2.23 Å (032), 2.17 Å (032), 2.12 Å, 2.02 Å, 1.94 Å, 1.90 Å (151), 1.87 Å (141), 1.83 Å, 1.74 Å (051), 1.71 Å (444), 1.69 Å (223), 1.66 Å, 1.62 Å, 1.59 Å (043), and 1.50 Å and 1.48 (233) (Fig. 3). Peaks at 2.08 and 1.81 Å (also present in the XRD pattern of the

saponite produced in the solution at pH 14; Fig. 1) were attributed to an austenitic steel from a spatula used during preparation for XRD. The FTIR spectrum (Fig. 4) shows two bands at 735 and 664 cm^{-1} corresponding to $\nu\text{Si-O-Si}$ and $\nu\text{Si-O-Al}$ vibrations, and a band at 613 cm^{-1} attributed to 4-membered rings vibrations of analcime (Mozgawa et al., 2011).

Nontronite Syntheses

Each of the syntheses conducted in solutions at pH of <13 produced red solid residues, with the exception of the syntheses conducted with the AlCl_3 solution at pH 10.6 and the syntheses conducted in solutions at pH 12.5 using the gels obtained with the AlCl_3 solutions above pH 5.4. The latter produced gelatinous solid residues that were green on top and orange below. In contrast, the syntheses conducted in solutions at pH 13 produced gelatinous solid residues green on top and yellow below.

Syntheses from the Gels Obtained using the AlCl_3 Solution at pH 3.4

Each of the four syntheses produced solid residues immersed in a reddish solution at a pH lower than that of the solution in which the starting gel was immersed (i.e. 4.7 for the synthesis conducted in pure water, 8.3 in the solution at pH 12, 10.7 at pH 12.5, and 12.7 at pH 13; Table 2). The XRD patterns of the synthetic products are very different from

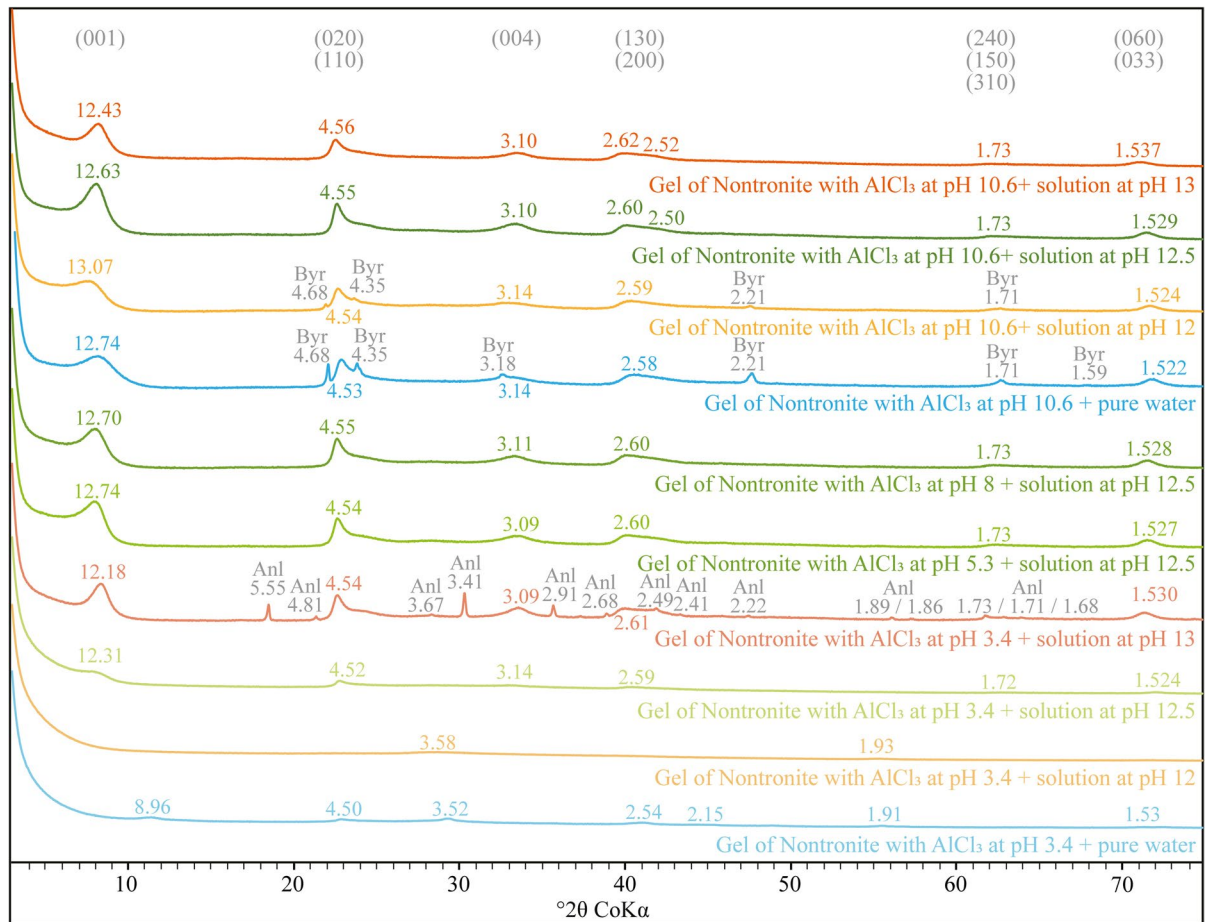


Fig. 5 XRD patterns of products of syntheses conducted with the gels of nontronite composition. Byr: Bayerite. Anl: Analcime

one another (Fig. 5). The solid produced in pure water exhibited XRD peaks at 8.96 Å (001), 4.50 Å (02,11), 3.52 Å (002), 2.54 Å (20,13), 2.32 Å (04,22), 2.15 Å, 1.91 Å, 1.53 Å (06,33), and 1.50 Å, probably corresponding to hisingerite (i.e. a precursor of nontronite containing no Al, nontronite-like phase; Eggleton, 1998; Farmer et al., 1994; Kohyama, 1975), while the solid produced in the solution at pH 12 exhibited only two broad bands near 3.58 and 1.93 Å, maybe indicating the presence of a semi-amorphous hisingerite). The solid produced in the solution at pH 12.5 showed a broad peak at ~12.3 Å (001) and weak peaks at 4.52 Å (02,11), 3.14 Å (004), 2.59 Å (13,20), 1.72 Å (15,24,31), and 1.524 Å (06,33) corresponding to nontronite (Baron et al., 2016a). The solid produced in the solution at pH 13 contained sharper, rather crystalline nontronite

(XRD peaks at 12.18 Å (001), 4.54 Å (02,11), 3.09 Å (004), 2.61 Å (13,21), and 1.530 Å (06,33); Fig. 5) mixed with analcime (XRD peaks at 5.55, 4.81, 3.67, 3.41, 2.91, 2.68, 2.49, 2.41, 2.22, 1.89, 1.86, 1.73, 1.71, and 1.68 Å; Fig. 5). Note that the 06,33 reflection of this nontronite was shifted toward lower angles (greater d spacings) possibly indicating $^{41}\text{Fe}^{3+}$ for $^{41}\text{Si}^{4+}$ tetrahedral substitutions and, thus, an increase of its charge (Baron et al., 2016a). The FTIR data (Fig. 6) confirmed the interpretations of the XRD patterns; the bands typical of nontronite (i.e. $\nu\text{Fe}_2^{3+}\text{-OH}$ at $\sim 3560\text{ cm}^{-1}$, $\delta\text{Fe}_2^{3+}\text{-OH}$ at 815 cm^{-1} , the 855 cm^{-1} (not assigned), $^{41}\text{Fe-O}$ at 707 cm^{-1} , and $^{61}\text{Fe}^{3+}\text{-O}_{\text{ap}}\sim 667\text{ cm}^{-1}$; Baron et al., 2016a; Dzene et al., 2022; Goodman et al., 1976) were stronger in the FTIR spectrum of the solid produced in the solution at pH 13 than in the FTIR spectrum of the

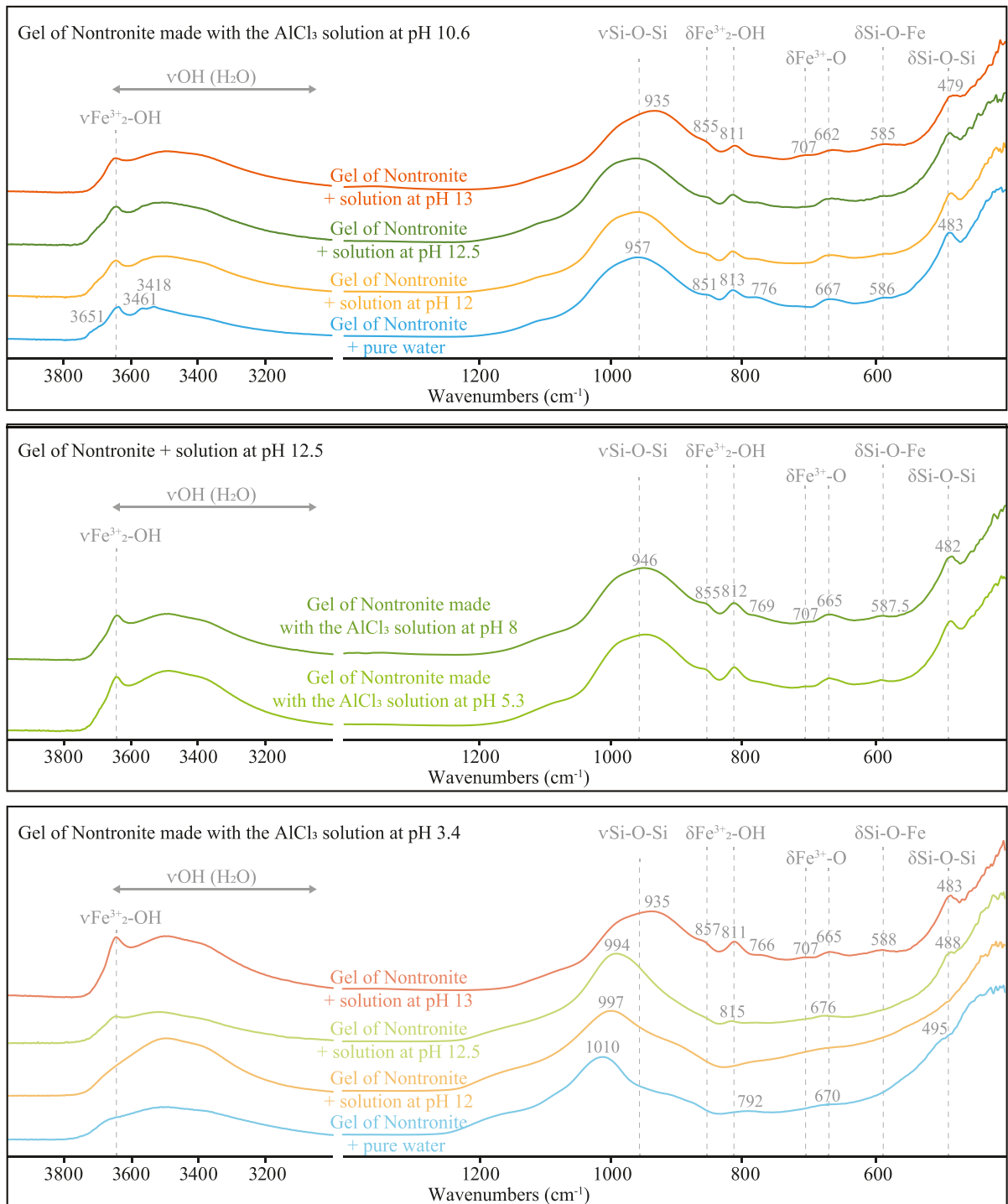


Fig. 6 FTIR spectra of products of syntheses conducted with the gels of nontronite composition

solid produced in the solution at pH 12.5, indicating that the nontronite produced at pH 12.5 was poorly crystallized. No band typical of nontronite was observed in the FTIR spectra of the solids produced in solutions at pH <12.5 (Fig. 6).

Syntheses from the Gels Obtained using the AlCl₃ Solution at pH 10.6

Each of the four syntheses produced solid residues immersed in solutions ranging from reddish to colorless; the lower the pH of the solution in which the synthesis was conducted, the more reddish the solution at the end of the synthesis (Table 2). With the exception of the final solution of the synthesis conducted in pure water at pH which ended at pH 9.7, the final solutions had pH values close to those of the solutions in which the starting gels were immersed (Table 2). The XRD patterns of all the solids show the presence of nontronite, i.e. XRD peaks at 12.43–13.07 Å (001), 4.53–4.56 Å (02,11), 3.10–3.14 Å (004), 2.58–2.62 Å (13,20), 1.73 Å (13,24,31), and 1.522–1.537 Å (06,33) (Baron et al., 2016a; Fig. 5). The increase of the 06,33 reflection position may indicate increasing ¹⁴Fe³⁺ for ¹⁴Si⁴ tetrahedral substitutions with increasing pH (Baron et al., 2016a). The additional presence of bay-erite (Al(OH)₃) can be inferred from the solid produced in pure water, as well as from the solid produced in the solution at pH 12 (although in lower abundance), from the XRD peaks at 4.68, 4.35, 3.18, 2.21, 1.71, and 1.59 Å (Lefevre & Fedoroff, 2002; Milligan, 1951) and the FTIR bands at 3651, 3545, 3461, and 3418 cm⁻¹ (Phambu et al., 2002 – Figs. 5 and 6). FTIR spectra of all solid residues showed bands typical of nontronite (i.e. bands at ~3560 cm⁻¹ (νFe₂OH), ~950 cm⁻¹ (νSi–O), ~815 cm⁻¹ (δFe³⁺₂OH), ~667 cm⁻¹ (¹⁶Fe³⁺–O_{ap}), 585 cm⁻¹ (δSi–O) and ~480 cm⁻¹ (¹⁶Fe–O–Si) (Baron et al., 2016a; Goodman et al., 1976). The bands at 850 and 707 cm⁻¹ are present commonly in nontronite with large ¹⁶Fe occupancy, but the band at 707 cm⁻¹ is present only in the FTIR spectrum of the nontronite produced in the solution at pH 13. Of note, the weak band at ~3635 cm⁻¹ observed in the FTIR spectra of the solids produced in the solutions at pH 12 and 12.5 corresponds to OH vibrations from water (cf Fig. S2). Under vacuum, the *d*₀₀₁ of the nontronite synthesized in the solution at pH 12 with the gel produced using the AlCl₃ solution at pH 10.6 collapsed to 10.06 Å (Fig. S1).

Syntheses from the Gels Obtained using the AlCl₃ Solutions at pH 5.3 and pH 8

Both syntheses conducted in the solution at pH 12.5 produced nontronite as revealed by XRD (peaks at ~12.7 Å, 4.55 Å / 4.54 Å, 3.1 Å, 2.6 Å, 1.73 Å, 1.528 Å / 1.527 Å; Baron et al., 2016a) and FTIR (bands at 3564, 812, 855, 707, and 665 cm⁻¹; Baron et al., 2016a; Goodman et al., 1976; Figs. 5 and 6). However, a band at 707 cm⁻¹, corresponding to ¹⁴Fe–O vibrations, is present in both FTIR spectra, probably indicating ¹⁴Fe³⁺ for ¹⁴Si⁴⁺ tetrahedral substitutions.

Discussion

The results show that the conditions required for the syntheses of pure (i.e. with no other mineral) Al-substituted smectite end-members (saponite, beidellite, and nontronite) are very different, even though these smectites differ only by the cation present at their octahedral sites. In this article the sensitivity to pH conditions of the production of pure saponite, beidellite, and nontronite is discussed and the various protocols leading to their successful syntheses are summarized.

Influence of pH

The results reported here show that the synthesis of pure saponite does not depend heavily on the pH of the solution in which the gels of saponite composition are immersed (saponite was obtained in solutions at pH ranging from 5.5 to 14). This can be due to the stability of the starting gel of trioctahedral smectites, as previously observed by Huertas et al. (2000). Of note, the saponites produced in the present study contain tetrahedral Al and no octahedral Al. In fact, the ATR-FTIR spectra of the saponites produced were very similar to the ATR-FTIR spectrum of saponite presented by Kloprogge and Ponce (2021), with a feature at 800–815 cm⁻¹ attributed to δAl–O of tetrahedral Al (absent from the ATR-FTIR spectrum of talc which contains no tetrahedral Al; Kloprogge & Ponce, 2021). Plus, the absence of the FTIR band attributed to νMg₂–Al–OH at 3625 cm⁻¹ is consistent with the absence of octahedral Al (Kloprogge & Ponce, 2021).

The XRD pattern of the saponite synthesized in solutions at pH 14 exhibited narrower 001 reflections than those of the saponites synthesized in solutions at lower pH. Such a decrease in width indicates a decrease in the d_{001} distance and can be interpreted as an increase in crystallinity (Zhang et al., 2022). Consistently, high-pH conditions during syntheses have been reported to improve both the crystallinity and crystallization rate of saponites (Blukis et al., 2022), as is the case for high-temperature conditions (Kloprogge & Frost, 2000; Kloprogge & Ponce, 2021). Still, such a decrease in width may also indicate an increase in the permanent charge, i.e. a higher degree of $^{[4]}Al^{3+}$ for $^{[4]}Si^{4+}$ tetrahedral substitutions. Consistently, with increasing pH (from 5.5 to 14), the $\nu Si-O-Si$ and $\delta Al-O$ absorption bands shifted from 960 to 944 cm^{-1} and from 800 to 815 cm^{-1} , respectively, while the νMg_3OH and δMg_3OH absorption bands of the synthesized saponites shifted from 3674 to 3685 cm^{-1} and from 655 to 640 cm^{-1} , respectively (Fig. 2), such shifts having been interpreted previously as an increase in the permanent charge (Meyer et al., 2020; Pelletier et al., 2003). Note that the production of saponites with a higher charge should leave available Si and Mg in the system, possibly leading to the production of other phases such as brucite ($Mg(OH)_2$), serpentine ($Mg_3Si_2O_5(OH)_4$), or talc ($Si_4Mg_3O_{10}(OH)_2$), i.e. an assemblage similar to what is obtained with a gel produced using Na_2SiO_3 and $AlCl_3$ solutions at pH 14 (Fig. S3). The absence of these minerals in the final residue (only saponite is present according to XRD and FTIR data; Figs. 1 and 2) suggests either that both Si and Mg in excess have been leached during filtration or that some Mg has replaced Na as the interlayer cation. Additional data (such as elemental or nuclear magnetic resonance – NMR data) would be required to determine if the saponite produced by immersing the gel in a solution at pH 14 has exactly the same composition as those produced at lower pH.

In contrast to that of saponite, the synthesis of beidellite is highly sensitive to the pH of the $AlCl_3$ solution and the pH of the solution in which gels are immersed. A gel of beidellite composition produced using an $AlCl_3$ solution at pH 3.4 seems to be very unstable and does not lead to the formation of pure beidellite, irrespective of the pH of the solution used for the synthesis (cf Fig. S4). In contrast, a gel of beidellite composition produced using an $AlCl_3$ solution

at pH 10.6 will lead systematically to the formation of boehmite (cf Fig. S4). Syntheses using gels of beidellite composition immersed in pure water will lead to the formation of kaolins, while only zeolites form in solutions at high pH, as also reported by De Kimpe (1976) and Huertas et al. (2000). The cause resides in the (pH-dependent) form of Si and Al species. In pure water, H_4SiO_4 , $Al(OH)_2^+$, and $Al(OH)^{2+}$ prevail, and Si and Al ions form tetrahedral and octahedral complexes, respectively, while at high pH (> 13), $H_2SiO_4^-$ and $Al(OH)_4^-$ prevail, leading to the formation of only tetrahedral complexes (Table 1). Thus, the successful synthesis of pure beidellite occurs only at a very specific pH (i.e. 12), where fourfold and sixfold coordinated Al species exist, as previously suggested (De Kimpe, 1976).

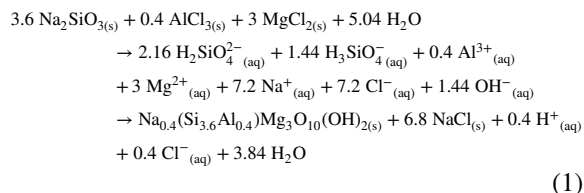
The synthesis of $^{[4]}Al$ -nontronite is also very sensitive to the pH of solutions, as is the case for $^{[4]}Fe$ -nontronite as acknowledged earlier (Andrieux & Petit, 2010; Boumaiza et al., 2020; Dzene et al., 2022). Only the gel produced using an $AlCl_3$ solution at pH 10.6 and immersed in a solution at pH 12.5 leads to pure $^{[4]}Al$ -nontronite. The syntheses conducted at pH < 12.5 from the gels of nontronite composition produced using an $AlCl_3$ solution at pH 10.6 led to the production of nontronite together with bayerite. Gels produced using an $AlCl_3$ solution at pH 10.6 and immersed in solutions at pH 13 crystallized into pure nontronite, but these are $^{[4]}Fe$ -nontronites as indicated by the shift of the 06,33 reflection to lower angles and the shift of the $\nu Si-O$ to lower wavelengths (Baron et al., 2016a). A high pH, thus, seems to favor $^{[4]}Fe^{3+}$ for $^{[4]}Si^{4+}$ tetrahedral substitutions, as historically suggested by Grubb (1969). The use of gels produced using an $AlCl_3$ solution at pH 3.4 did not lead to the production of pure, well crystallized $^{[4]}Al$ -nontronite (only poorly crystalline nontronite is obtained at pH 12.5). The immersion of such gels in solutions at lower pH leads to the production of hisingerite (i.e. a precursor of nontronite containing no Al; Kohyama, 1975; Farmer et al., 1994; Eggleton, 1998; Milliken & Bish, 2014), while their immersion in solutions at higher pH leads to the production of a zeolite (analcime) together with $^{[4]}Fe$ -nontronite.

Mechanistic Considerations

This section concerns the reactions that have probably occurred during the syntheses of saponite, beidellite,

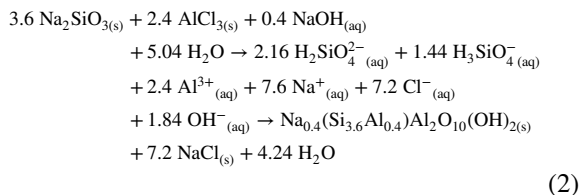
and nontronite. Please note that the equations presented below refer to the theoretical products of the syntheses carried out in the present study.

Pure saponite can be synthesized following various protocols, at various temperatures (Kloprogge & Frost, 2000; Meyer et al., 2020) and for different durations (Zhang et al., 2020), whatever the pH (Blukis et al., 2022). Here, saponite was obtained by immersing gels in solutions at pH ranging from 5.5 to 14, probably because the rather large Mg^{2+} ions did not compete with Al species for tetrahedral substitutions. The major species in the Na_2SiO_3 solution at 0.2 M at pH 13.1 are $H_2SiO_4^{2-}$ and $H_3SiO_4^-$ (Table 1). Although Al was present mainly as Al^{3+} in the $AlCl_3$ solution, it converted to $Al(OH)_4^-$ when this solution was poured into the Na_2SiO_3 solution, leading to the polymerization of an aluminosilicate network (i.e. tetrahedral complexes) at high pH (as suggested by Beselink et al., 2020). The subsequent addition of the $MgCl_2$ solution was responsible for a slight decrease in the pH (down to 10 – Table 2), probably converting the remaining $H_2SiO_4^{2-}$ ions into $H_3SiO_4^-$, thereby leading to the polymerization of Mg-rich octahedral complexes. The gel produced crystallized into saponite whatever the pH of the solution into which it will be immersed, following the overall simplified reaction, written with respect to the main species present in each starting solution at 20°C (cf Table 1).

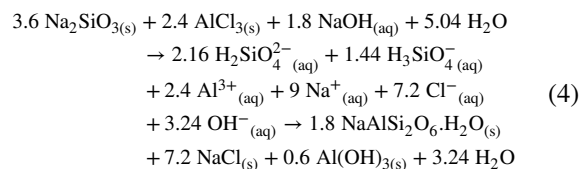
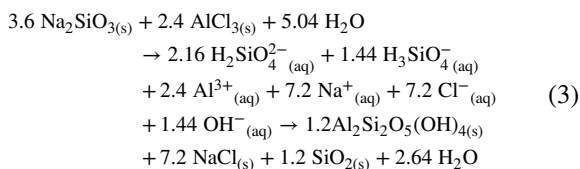


Pure beidellite cannot be synthesized over a large range of pH. The pH of the solution in which the gel is immersed for crystallization has to be controlled precisely. Although the formation of tetrahedral complexes occurred as for saponite when pouring the $AlCl_3$ solution at pH 3.9 into the Na_2SiO_3 solution at 0.2 M at pH 13.1, the subsequent addition of the second $AlCl_3$ solution was responsible for a large decrease in the pH (down to 4.5 – Table 2), destabilizing the tetrahedral complexes already formed and converting the $H_2SiO_4^{2-}$ ions into H_4SiO_4 and the $Al(OH)_4^-$ ions into $Al(OH)_2^+$, $Al(OH)^{2+}$, and Al^{3+} . The gel obtained with the starting $AlCl_3$ solution at pH 3.9 will crystallize into pure beidellite only if

immersed in solutions at pH 12 (allowing the conversion of Al species into $Al(OH)_4^-$, and thus the incorporation of tetrahedral Al) followed the overall simplified reaction, written with respect to the main species present in each starting solution at 20°C (cf Table 1):

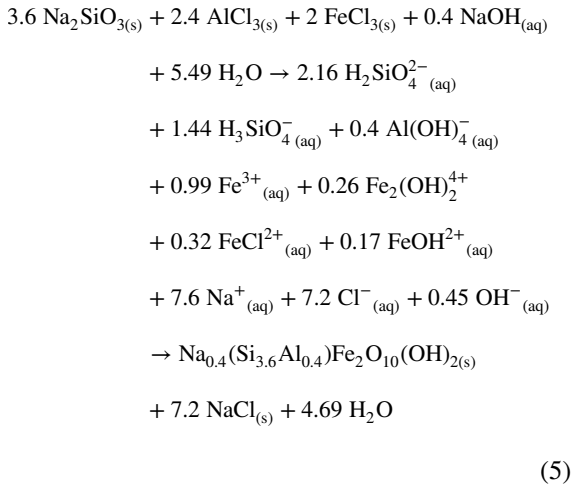


If the gel is immersed in a solution at pH <12, only kaolins will be produced following Eq. 3, while if the gel is immersed in a solution at pH >12, only zeolites will be produced following Eq. 4 (together with SiO_2 or $Al(OH)_3$, respectively, which are probably leached during filtration). Note that a starting $AlCl_3$ solution at pH >8, which would contain $Al(OH)_4^-$ ions, cannot be used to produce a gel because of the inevitable precipitation of $AlOOH$ or $Al(OH)_3$ (Fig. S4).



Pure nontronite cannot be synthesized over a large pH range. As for beidellite, the pH of the solution in which the gel is immersed for crystallization has to be controlled precisely, even though the pH of the starting $AlCl_3$ solution does not seem to be critical, given that pure $^{[4]}Fe$ -nontronite or $^{[4]}Al$ -nontronite were produced here from $AlCl_3$ solutions at either pH 3.4 or 10.6. However, here, only the use of an $AlCl_3$ solution at pH 10.6 led to the production of $^{[4]}Al$ -Nontronite. As for saponite and beidellite, the formation of tetrahedral complexes occurred when pouring the $AlCl_3$ solution into the 0.2 M Na_2SiO_3 solution at pH 13.1. The subsequent addition of the $FeCl_3$ solution was responsible for only a slight decrease in the pH (down to 9; Table 2), leading to the production of

Fe-rich octahedral complexes forming a gel which would crystallize into pure $^{[4]}\text{Al}$ -nontronite only if immersed in solutions at pH 12.5 following the overall simplified reaction, written with respect to the main species present in each starting solution at 20°C (cf Table 1):



At high pH, the major species in solution were H_3SiO_4^- , $\text{H}_2\text{SiO}_4^{2-}$, $\text{Al}(\text{OH})_4^-$, and $\text{Fe}(\text{OH})_4^-$ (Guan et al., 2009; Perry & Shafran, 2001), with $\text{Al}(\text{OH})_4^-$ competing with $\text{Fe}(\text{OH})_4^-$ for tetrahedral substitutions (Decarreau & Petit, 2014). According to the present results, if the gel is immersed in a solution at pH 12.5, $\text{Al}(\text{OH})_4^-$ is preferentially incorporated into tetrahedral sites over $\text{Fe}(\text{OH})_4^-$, leading eventually to the production of $^{[4]}\text{Al}$ -nontronite. In contrast, if the gel is immersed in a solution at pH >12.5, $\text{Fe}(\text{OH})_4^-$ is incorporated preferentially into tetrahedral sites over $\text{Al}(\text{OH})_4^-$, eventually leading to the production of $^{[4]}\text{Fe}$ -nontronite rather than $^{[4]}\text{Al}$ -nontronite (cf Fig. 6). At pH <12.5, Al seems to be incorporated neither in tetrahedral nor octahedral sites and bayerite is produced together with $^{[4]}\text{Fe}$ -nontronite (Fig. 6).

Concluding Remarks

Optimal pH for the Synthesis of Saponite, Beidellite, and Nontronite

The successful synthesis of saponite was achieved by exposing the starting gels to a temperature of 230°C for 4 days in solutions at pH ranging from 5.5 to 14, confirming the pH non-sensitivity of saponite

production (Blukis et al., 2022). Of note, the gel-to-solution ratio is an important parameter. Here, a mass of ~100 mg of gel was immersed in 16.5 mL of solution. In a similar volume of solution, a smaller (50 mg) or a larger (200 mg) mass of gel led to the formation of less crystalline saponites (data not shown here).

The successful synthesis of beidellite was achieved by exposing the gel obtained using the AlCl_3 solution at pH 3.9 to 230°C for 9 days in a solution at pH 12. The gel-to-solution ratio is also an important parameter. Here, a mass of about 80 mg of gel was immersed into 12.5 mL of solution at pH 12. In a similar volume of solution, a lower mass of gel (60 mg) led to the formation of zeolites, while a larger mass of gel (100 mg) led to the formation of kaolins and aluminum hydroxides (data not shown here).

The successful synthesis of nontronite was achieved by exposing the starting gels to 150°C for 2.5 days in solutions at pH between 12.5 and 13. Pure nontronite was obtained by immersing gels prepared with an AlCl_3 solution at a pH above 5 in solutions at pH 12.5 (confirming the results of Andrieux & Petit, 2010). Here, a mass of ~165 mg of gel was immersed in 16.5 mL of solution. Of note, changing this ratio will influence the pH and may lead to the additional production of either analcime or aluminum hydroxides (data not shown here).

Implications for Natural Systems

Smectites carry key information on the geochemistry, oxidation state, and water content of the environments in which they were produced (Ehlmann et al., 2011; Fox et al., 2021), making them good indicators of paleoenvironmental and paleoclimatic conditions. Although further characterization (such as elemental or NMR analyses) would be required to ascertain the exact structure and composition of the various products more precisely, the present study shows that the optimal pH for the synthesis of saponite, beidellite, or nontronite is different; pH conditions influence strongly the purity and the final crystallochemistry of the smectites produced. Although extrapolating experimental results to natural settings remains complicated, the present results suggest that the crystallochemistry of natural smectites could also be used (a priori) as a paleo-pH proxy. However, smectitic clay minerals are rarely pure in natural settings, and most often exist in a complicated assemblage of various

(more or less interstratified) clay mineral phases. Plus, natural clay minerals, either terrestrial or extraterrestrial, have usually experienced a complex history, including possible transport, mixing, reworking, and alteration, without mentioning interactions with organic compounds which may influence the crystallization and the final crystallochemistry of clay minerals (Jacquemot et al., 2019; Viennet et al., 2019, 2022). Finally, the precise estimation of an age is fundamental for a proxy to be useful, and it remains very difficult to date smectitic clay minerals other than relying on certain impurities (transition ions) and point defects (radicals) which may be probed using electron paramagnetic resonance spectroscopy (Allard et al., 2012; Balan et al., 2020). Still, there is no doubt that the results of the present study will be of great help to constrain better the geochemical conditions existing or having existed on extraterrestrial planetary bodies such as Mars, on which the production of clay minerals has been intense (Carter et al., 2013; Ehlmann & Edwards, 2014), or on rocky and/or icy small bodies such as Ceres, Enceladus, or Europa on which the production of (probably smectitic) clay minerals have recently been reported (Marchi et al., 2019; Nordheim et al., 2018; Waite et al., 2017).

Acknowledgements The authors acknowledge the spectroscopic and X-ray diffraction facilities of the Institut de Minéralogie, de Physique des Matériaux et de Cosmochimie (IMPMC) and Elisabeth Malassis for administrative support.

Authors' Contributions IC, JCV, and SB designed the present study. IC and JCV performed the FTIR and the XRD analyses, with the help of LD and MG. All authors contributed to the interpretation of the data and discussed their implications. IC, JCV, and SB wrote the present manuscript, with critical inputs from FB, AB, and EB.

Funding This work was made possible thanks to financial support from the ATM program at MNHN (Project BioMars; PI: S. Bernard), from the Institut des Matériaux de Sorbonne Université (IMat) (Project Ageing on Mars; PI: S. Bernard) and from the European Research Council (ERC Consolidator Grant No. 819587: HYDROMA; PI: L. Remusat).

Data Availability All data are available at <https://drive.google.com/drive/folders/1prbEh1-XBEL-Qcb8NxxvS1qzryqQ873yZ?usp=sharing>

Declarations

Conflicts of Interest The authors declare that they have no known competing financial interests or personal relationships that could have appeared to influence the work reported in this article.

References

- Abbott, A. N., Löhr, S., & Trethewey, M. (2019). Are clay minerals the primary control on the oceanic rare earth element budget? *Frontiers in Marine Science*, 6, 504.
- Abdo, J., & Haneef, M. D. (2013). Clay nanoparticles modified drilling fluids for drilling of deep hydrocarbon wells. *Applied Clay Science*, 86, 76–82.
- Abdulelah, H., Keshavarz, A., Hoteit, H., Abid, H., Goudeli, E., Ennis-King, J., & Iglauer, S. (2023). Hydrogen physisorption in earth-minerals: Insights for hydrogen subsurface storage. *Journal of Energy Storage*, 66, 107440.
- Allard, T., Balan, E., Calas, G., Fourdrin, C., Morichon, E., & Sorieul, S. (2012). Radiation-induced defects in clay minerals: A review. *Nuclear Instruments and Methods in Physics Research B*, 277, 112–120.
- Almqvist, B. S. G., & Mainprice, D. (2017). Seismic properties and anisotropy of the continental crust: Predictions based on mineral texture and rock microstructure. *Reviews of Geophysics*, 55, 367–433.
- Andrieux, P., & Petit, S. (2010). Hydrothermal synthesis of dioctahedral smectites: The Al-Fe³⁺ chemical series. *Applied Clay Science*, 48, 5–17.
- Balan, E., Allard, T., Morin, G., Fritsch, E., & Calas, G. (2020). Crystallochemistry of clay minerals, weathering processes and evolution of continental surfaces. In P. Bertrand (Ed.) *Electron paramagnetic resonance spectroscopy* (pp. 109–135). Springer, Cham. https://doi.org/10.1007/978-3-030-39668-8_5
- Baron, F., Petit, S., Tertre, E., & Decarreau, A. (2016a). Influence of aqueous si and fe speciation on tetrahedral fe(III) substitutions in nontronites: a clay synthesis approach. *Clays and Clay Minerals*, 64, 230–244.
- Baron, F., Pushparaj, S. S. C., Fontaine, C., Sivaiah, M. V., Decarreau, A., & Petit, S. (2016). Microwave-assisted hydrothermal synthesis of Ni-Mg layered silicate clays. *Current Microwave Chemistry*, 3, 85–89.
- Bello, M. L., Junior, A. M., Freitas, C. A., Moreira, M. L. A., da Costa, J. P., de Souza, M. A., Santos, B. A. M. C., de Sousa, V. P., Castro, H. C., Rodrigues, C. R., & Cabral, L. M. (2022). Development of novel montmorillonite-based sustained release system for oral bromopride delivery. *European Journal of Pharmaceutical Sciences*, 175, 106222.
- Besselink, R., Stawski, T. M., Freeman, H. M., Hövelmann, J., & To, D. J. (2020). Mechanism of saponite crystallization from a rapidly formed amorphous intermediate. *Crystal Growth & Design*, 20(5), 3365–3373.
- Blattmann, T. M., Liu, Z., Zhang, Y., Zhao, Y., Haghipour, N., Montluçon, D. B., Plötze, M., & Eglinton, T. I. (2019). Mineralogical control on the fate of continentally derived organic matter in the ocean. *Science*, 366, 742–745.
- Blukis, R., Schindler, M., Couason, T., & Benning, L. G. (2022). Mechanism and control of saponite synthesis from a self-assembling nanocrystalline precursor. *Langmuir*, 38, 7678–7688.
- Boonruang, C., & Sanumang, W. (2021). Effect of nano-grain carbide formation on electrochemical behavior of 316L stainless steel. *Scientific Reports*, 11, 12602.
- Boumaiza, H., Dutournié, P., Le Meins, J.-M., Limousy, L., Brendlé, J., Martin, C., Michau, N., & Dzene, L. (2020).

- Iron-rich clay mineral synthesis using design of experiments approach. *Applied Clay Science*, 199, 105876. <https://doi.org/10.1016/j.clay.2020.105876>
- Brown, G., & Brindley, G. W. (1980) X-ray diffraction procedures for clay mineral identification. In G. W. Brindley & G. Brown (Eds.), *Crystal structures of clay minerals and their x-ray identification*. Mineralogical Society of Great Britain and Ireland.
- Carniato, F., Gatti, G., & Bisio, C. (2020). An overview of the recent synthesis and functionalization methods of saponite clay. *New Journal of Chemistry*, 44, 9969–9980.
- Carretero, M. I., & Pozo, M. (2009). Clay and non-clay minerals in the pharmaceutical industry. *Applied Clay Science*, 46, 73–80.
- Carroll, D. (1970). Clay minerals: a guide to their X-ray identification. *Special Papers of the Geological Society of America*, 126, 1–81. <https://doi.org/10.1130/SPE126>
- Carter, J., Poulet, F., Bibring, J. P., Mangold, N., & Murchie, S. (2013). Hydrous minerals on mars as seen by the CRISM and OMEGA imaging spectrometers: updated global view. *Journal of Geophysical Research: Planets*, 118, 831–858.
- Choy, J.-H., Choi, S.-J., Oh, J.-M., & Park, T. (2007). Clay minerals and layered double hydroxides for novel biological applications. *Applied Clay Science*, 36, 122–132.
- Churchman, G. J., Gates, W. P., Theng, B. K. G., & Yuan, G. (2006) Clays and clay minerals for pollution control. In F. Bergaya, B.K.G. Theng, G. Lagaly (Eds.), *Developments in Clay Science* (pp. 625–675). Amsterdam: Elsevier. [https://doi.org/10.1016/S1572-4352\(05\)01020-2](https://doi.org/10.1016/S1572-4352(05)01020-2)
- Corbin, G., Vulliet, E., Lanson, B., Rimola, A., & Mignon, P. (2021). Adsorption of pharmaceuticals onto smectite clay minerals: a combined experimental and theoretical study. *Minerals*, 11, 62.
- de Jong, S. M., Spiers, C. J., & Busch, A. (2014). Development of swelling strain in smectite clays through exposure to carbon dioxide. *International Journal of Greenhouse Gas Control*, 24, 149–161.
- de Mello Gabriel, G. V., Machado Pitombo, L., Tavares Rosa, L. M., AparecidoNavarrete, A., Botero, W. G., do Carmo, J. B., & Camargo de Oliveira, L. (2021). The environmental importance of iron speciation in soils: evaluation of classic methodologies. *Environmental Monitoring and Assessment*, 193, 63.
- De Kimpe, C. R. (1976). Formation of phyllosilicates and zeolites from pure silica-alumina gels. *Clays and Clay Minerals*, 24, 200–207.
- Decarreau, A., & Petit, S. (2014). Fe³⁺/Al³⁺ partitioning between tetrahedral and octahedral sites in dioctahedral smectites. *Clay Minerals*, 49, 657–665.
- Decarreau, A., Grauby, O., & Petit, S. (1992). The actual distribution of octahedral cations in 2:1 clay minerals: results from clay synthesis. *Applied Clay Science*, 7, 147–167.
- Decarreau, A., Petit, S., Martin, F., Farges, F., Vieillard, P., & Joussein, E. (2008). Hydrothermal synthesis, between 75 and 150°C, of high-charge, ferric nontronites. *Clays and Clay Minerals*, 56, 322–337.
- Delage, P., Cui, Y. J., & Tang, A. M. (2010). Clays in radioactive waste disposal. *Journal of Rock Mechanics and Geotechnical Engineering*, 2, 111–123.
- Delvaux, B., Mestdagh, M. M., Vielvoye, L., & Herbillon, A. J. (1989). XRD, IR and ESR study of experimental alteration of Al-nontronite into mixed-layer kaolinite/smectite. *Clay Minerals*, 24, 617–630.
- Dzene, L., Brendlé, J., Limousy, L., Dutournié, P., Martin, C., & Michau, N. (2018). Synthesis of iron-rich tri-octahedral clay minerals: A review. *Applied Clay Science*, 166, 276–287.
- Dzene, L., Dutournié, P., Brendlé, J., Limousy, L., Le Meins, J.-M., Michelin, L., Vidal, L., Gree, S., Abdelmoula, M., Martin, C., & Michau, N. (2022). Characterization of iron-rich phyllosilicates formed at different Fe/Si ratios. *Clays and Clay Minerals*, 70, 580–594.
- Eggleton, R. A. (1998). Hisingerite: a ferric kaolin mineral with curved morphology. *Clays and Clay Minerals*, 46, 400–413.
- Ehlmann, B. L., & Edwards, C. S. (2014). Mineralogy of the Martian surface. *Annual Review of Earth and Planetary Sciences*, 42(1), 291–315.
- Ehlmann, B. L., Mustard, J. F., Clark, R. N., Swayze, G. A., & Murchie, S. L. (2011). Evidence for low-grade metamorphism, hydrothermal alteration, and diagenesis on Mars from phyllosilicate mineral assemblages. *Clays and Clay Minerals*, 59, 359–377.
- Ewis, D., Ba-Abbad, M. M., Benamor, A., & El-Naas, M. H. (2022). Adsorption of organic water pollutants by clays and clay minerals composites: A comprehensive review. *Applied Clay Science*, 229, 106686.
- Farmer, V. C. (1974). *The infrared spectra of minerals*. Mineralogical Society.
- Farmer, V. C., & Russell, J. D. (1964). The infra-red spectra of layer silicates. *Spectrochimica Acta*, 20, 1149–1173.
- Farmer, V. C., McHardy, W. J., Elsass, F., & Robert, M. (1994). hk-ordering in aluminous nontronite and saponite synthesized near 90°C: effects of synthesis conditions on nontronite composition and ordering. *Clays and Clay Minerals*, 42, 180–186.
- Ferrage, E., Lanson, B., Sakharov, B. A., & Drits, V. A. (2005). Investigation of smectite hydration properties by modeling experimental X-ray diffraction patterns: Part I. Montmorillonite Hydration Properties. *American Mineralogist*, 90, 1358–1374.
- Ferrage, E., Lanson, B., Sakharov, B. A., Geoffroy, N., Jacquot, E., & Drits, V. A. (2007). Investigation of dioctahedral smectite hydration properties by modeling of X-ray diffraction profiles: Influence of layer charge and charge location. *American Mineralogist*, 92, 1731–1743.
- Fox, V. K., Kupper, R. J., Ehlmann, B. L., Catalano, J. G., Razzell-Hollis, J., Abbey, W. J., Schild, D. J., Nickerson, R. D., Peters, J. C., Katz, S. M., & White, A. C. (2021). Synthesis and characterization of Fe(III)-Fe(II)-Mg-Al smectite solid solutions and implications for planetary science. *American Mineralogist*, 106, 964–982.
- Ghadiri, M., Chrzanowski, W., & Rohanizadeh, R. (2015). Biomedical applications of cationic clay minerals. *RSC Advances*, 5, 29467–29481.
- Goodman, B. A., Russell, J. D., Fraser, A. R., & Woodhams, F. W. D. (1976). A Mössbauer and I.R. spectroscopic study of the structure of nontronite. *Clays and Clay Minerals*, 24, 53–59.
- Grauby, O., Petit, S., Decarreau, A., & Baronnet, A. (1993). The beidellite-saponite series: an experimental approach. *European Journal of Mineralogy*, 5, 623–636.

- Grauby, O., Petit, S., Decarreau, A., & Baronnet, A. (1994). The nontronite-saponite series: an experimental approach. *European Journal of Mineralogy*, *6*, 99–112.
- Grubb, P. L. C. (1969). Phase changes in aged sesquioxide gels and some analogies with katamorphic processes. *Mineralium Deposita*, *4*, 30–51.
- Guan, X., Dong, H., Ma, J., & Jiang, L. (2009). Removal of arsenic from water: effects of competing anions on As(III) removal in KMnO₄-Fe(II) process. *Water Research*, *43*, 3891–3899.
- Harder, H. (1976). Nontronite synthesis at low temperatures. *Chemical Geology*, *18*, 169–180.
- Hazen, R. M., Sverjensky, D. A., Azzolini, D., Bish, D. L., Elmore, S. C., Hinnov, L., & Milliken, R. E. (2013). Clay mineral evolution. *American Mineralogist*, *98*, 2007–2029.
- Ho, T. A., Jove-Colon, C. F., & Wang, Y. (2023). Low hydrogen solubility in clay interlayers limits gas loss in hydrogen geological storage. *Sustainable Energy & Fuels*, *7*, 3232–3238.
- Huertas, F. J., Cuadros, J., Huertas, F., & Linares, J. (2000). Experimental study of the hydrothermal formation of smectite in the beidellite-saponite series. *American Journal of Science*, *300*, 504–527.
- Hwang, H., Seoung, D., Lee, Y., Liu, Z., Liermann, H.-P., Cynn, H., Vogt, T., Kao, C.-C., & Mao, H.-K. (2017). A role for subducted super-hydrated kaolinite in earth's deep-water cycle. *Nature Geoscience*, *10*, 947–953.
- Ikari, M. J., Saffer, D. M., & Marone, C. (2009). Frictional and hydrologic properties of clay-rich fault gouge. *Journal of Geophysical Research: Solid Earth*, *114*, B05409.
- Jacquemot, P., Viennet, J. C., Bernard, S., Le Guillou, C., Rigaud, B., Delbes, L., Georgelin, T., & Jaber, M. (2019). The degradation of organic compounds impacts the crystallization of clay minerals and vice versa. *Scientific Reports*, *9*, 20251.
- Kalo, H., Möller, M. W., Ziadeh, M., Dolejš, D., & Breu, J. (2010). Large scale melt synthesis in an open crucible of Na-fluorohectorite with superb charge homogeneity and particle size. *Applied Clay Science*, *48*, 39–45.
- Katayama, I., Kubo, T., Sakuma, H., & Kawai, K. (2015). Can clay minerals account for the behavior of non-asperity on the subducting plate interface? *Progress in Earth and Planetary Science*, *2*, 30.
- Kennedy, M. J., Pevear, D. R., & Hill, R. J. (2002). Mineral surface control of organic carbon in black shale. *Science*, *295*, 657–660.
- Klopprogge, J. T. (1999). Synthesis of smectite clay minerals: a critical review. *Clays and Clay Minerals*, *47*, 529–554.
- Klopprogge, J. T., & Frost, R. L. (2000). The effect of synthesis temperature on the FT-Raman and FT-IR spectra of saponites. *Vibrational Spectroscopy*, *23*, 119–127.
- Klopprogge, J. T., & Hartman, H. (2022). Clays and the origin of life: the experiments. *Life*, *12*, 259.
- Klopprogge, J. T., & Ponce, C. P. (2021). Spectroscopic studies of synthetic and natural saponites: a review. *Minerals*, *11*, 112.
- Klopprogge, J. T., Jansen, J. B. H., & Geus, J. W. (1990). Characterization of synthetic Na-Beidellite. *Clays and Clay Minerals*, *38*, 409–414.
- Klopprogge, J. T., van der Eerden, A. M. J., Jansen, J. B. H., Geus, J. W., & Schuiling, R. D. (1993). Synthesis and paragenesis of Na-Beidellite as a function of temperature, water pressure, and sodium activity. *Clays and Clay Minerals*, *41*, 423–430.
- Kodama, H. (1962). Identification of kaolin minerals in the presence of chlorite by X-ray diffraction and infrared absorption spectra. *Clays and Clay Minerals*, *11*, 236–249.
- Kohyama, N. (1975). Hisingerite occurring as a weathering product of iron-rich saponite. *Clays and Clay Minerals*, *23*, 215–218.
- Komadel, P., Madejová, J., & Bujdák, J. (2005). Preparation and properties of reduced-charge smectites - a review. *Clays and Clay Minerals*, *53*, 313–334.
- Landais, P., Dohrmann, R., & Kaufhold, S. (2013). Overview of the clay mineralogy studies presented at the 'Clays in natural and engineered barriers for radioactive waste confinement' meeting, Montpellier, October 2012. *Clay Minerals*, *48*, 149–152.
- Lantenais, S., Muller, F., Bény, J.-M., Mahiaoui, J., & Champallier, R. (2008). Hydrothermal synthesis of beidellites: Characterization and study of the cis- and trans-vacant character. *Clays and Clay Minerals*, *56*, 39–48.
- Lefevre, G., & Fedoroff, M. (2002). Synthesis of bayerite (β -Al(OH)₃) microrods by neutralization of aluminate ions at constant pH. *Materials Letters*, *56*(6), 978–983.
- Li, K., Wang, Q., Ma, H., Huang, H., Lu, H., & Peng, P. (2023). Effect of clay minerals and rock fabric on hydrocarbon generation and retention by thermal pyrolysis of Maoming oil shale. *Processes*, *11*, 894.
- Madejová, J., Gates, W.P., & Petit, S. (2017). IR Spectra of Clay Minerals. In: *Developments in Clay Science*. Elsevier, pp. 107–149.
- Marchi, S., Raponi, A., Prettyman, T. H., Sanctis, M. C. D., Castillo-Rogez, J., Raymond, C. A., Ammannito, E., Bowling, T., Ciarniello, M., Kaplan, H., Palomba, E., Russell, C. T., Vinogradoff, V., & Yamashita, N. (2019). An aqueously altered carbon-rich Ceres. *Nature Astronomy*, *3*, 140.
- Meunier, A. (2005). *Clays*. Springer-Verlag, Berlin.
- Meunier, A., Mas, A., Beaufort, D., Patrier, P., & Dudoignon, P. (2008). Clay minerals in basalt-hawaiiite rocks from Mururoa atoll (French Polynesia). II. Petrography and Geochemistry. *Clays and Clay Minerals*, *56*, 730–750.
- Meyer, S., Bennici, S., Vaulot, C., Rigolet, S., & Dzene, L. (2020). Influence of the precursor and the temperature of synthesis on the structure of saponite. *Clays and Clay Minerals*, *68*, 544–552.
- Millero, F. J., Yao, W., & Aicher, J. (1995). The speciation of Fe(II) and Fe(III) in natural waters. *Marine Chemistry*, *50*(1–4), 21–39.
- Milligan, W. O. (1951). Recent X-ray diffraction studies on the hydrous oxides and hydroxides. *The Journal of Physical Chemistry*, *55*, 497–507.
- Milliken, R. & Bish, D. (2014). *Distinguishing hisingerite from other clays and its importance for Mars*. 45th Lunar and Planetary Science Conference, 2251.
- Moldoveanu, G. A., & Papangelakis, V. G. (2012). Recovery of rare earth elements adsorbed on clay minerals: I. *Desorption Mechanism*. *Hydrometallurgy*, *117–118*, 71–78.

- Mozgawa, W., Krol, M., & Barczyk, K. (2011). FT-IR studies of zeolites from different structural groups. *Chemik*, 65, 667–674.
- Murray, H. H. (1991). Overview - clay mineral applications. *Applied Clay Science*, 5, 379–395.
- Murray, H. H. (2000). Traditional and new applications for kaolin, smectite, and palygorskite: a general overview. *Applied Clay Science*, 17, 207–221.
- Nakazawa, H., Yamada, H., & Fujita, T. (1992). Crystal synthesis of smectite applying very high pressure and temperature. *Applied Clay Science*, 6, 395–401.
- Nordheim, T. A., Hand, K. P., & Paranicas, C. (2018). Preservation of potential biosignatures in the shallow subsurface of Europa. *Nature Astronomy*, 2, 673.
- Oleksiak, M. D., Ghorbanpour, A., Conato, M. T., McGrail, B. P., Grabow, L. C., Motkuri, R. K., & Rimer, J. D. (2016). Synthesis strategies for ultrastable zeolite gis polymorphs as sorbents for selective separations. *Chemistry - A European Journal*, 22, 16078–16088.
- Parrotin, F., Robin, V., Beaucaire, C., Descostes, M., & Tertre, E. (2023). Competitive ion-exchange reactions of Pb(II) ($Pb^{2+}/PbCl^+$) and Ra(II) (Ra^{2+}) on smectites: experiments, modeling, and implication for $^{226}Ra(II)/^{210}Pb(II)$ disequilibrium in the environment. *Chemosphere*, 313, 137369.
- Pelletier, M., Michot, L. J., Humbert, B., Barrès, O., de la Caillerie, J. B. D., & Robert, J. L. (2003). Influence of layer charge on the hydroxyl stretching of trioctahedral clay minerals: a vibrational study of synthetic Na- and K-saponites. *American Mineralogist*, 88, 1801–1808.
- Perry, C. C., & Shafran, K. L. (2001). The systematic study of aluminium speciation in medium concentrated aqueous solutions. *Journal of Inorganic Biochemistry*, 87(1–2), 115–124.
- Petit, S., Decarreau, A., Gates, W., Andrieux, P., & Grauby, O. (2015). Hydrothermal synthesis of dioctahedral smectites: the Al-Fe³⁺ chemical series. Part II: Crystal-Chemistry. *Applied Clay Science*, 104, 96–105.
- Petit, S., Baron, F., & Decarreau, A. (2017). Synthesis of nontronite and other Fe-rich smectites: a critical review. *Clay Minerals*, 52, 469–483.
- Phambu, N., Humbert, B., & Burneau, A. (2002). Use of diffuse reflectance infrared spectroscopy to monitor purification. *Journal of Chemical Education*, 79(9), 1117.
- Pierrot, D., & Millero, F. J. (2017). The speciation of metals in natural waters. *Aquatic Geochemistry*, 23, 1–20.
- Ponce, C. P., & Klopogge, J. T. (2020). Urea-assisted synthesis and characterization of saponite with different octahedral (Mg, Zn, Ni, Co) and tetrahedral metals (Al, Ga, B), a review. *Life*, 10, 168.
- Robin, V., Tertre, E., Beaucaire, C., Regnault, O., & Descostes, M. (2017). Experimental data and assessment of predictive modeling for radium ion-exchange on beidellite, a swelling clay mineral with a tetrahedral charge. *Applied Geochemistry*, 85, 1–9.
- Romanov, V. N. (2013). Evidence of irreversible CO₂ intercalation in montmorillonite. *International Journal of Greenhouse Gas Control*, 14, 220–226.
- Rother, G., Ilton, E. S., Wallacher, D., Hauß, T., Schaefer, H. T., Qafoku, O., Rosso, K. M., Felmy, A. R., Krukowski, E. G., Stack, A. G., Grimm, N., & Bodnar, R. J. (2013). CO₂ sorption to subsingle hydration layer montmorillonite clay studied by excess sorption and neutron diffraction measurements. *Environmental Science & Technology*, 47, 205–211.
- Saadat, S., Rawtani, D., & Parikh, G. (2022). Clay minerals-based drug delivery systems for anti-tuberculosis drugs. *Journal of Drug Delivery Science and Technology*, 76, 103755.
- Salter, T. L., Watson, J. S., & Sephton, M. A. (2023). Effects of minerals (phyllosilicates and iron oxides) on the responses of aliphatic hydrocarbon containing kerogens (Type I and Type II) to analytical pyrolysis. *Journal of Analytical and Applied Pyrolysis*, 170, 105900.
- See, K. A., Chapman, K. W., Zhu, L., Wiaderek, K. M., Borkiewicz, O. J., Barile, C. J., Chupas, P. J., & Gewirth, A. A. (2015). The interplay of Al and Mg speciation in advanced Mg battery electrolyte solutions. *Journal of the American Chemical Society*, 138, 328–337.
- Singh, N. B. (2022). Clays and clay minerals in the construction industry. *Minerals*, 12, 301.
- Tamura, K. (2000). Stepwise hydration of high-quality synthetic smectite with various cations. *Clays and Clay Minerals*, 48, 400–404.
- Tayraukham, P., Jantarit, N., Osakoo, N., & Wittayakun, J. (2020). Synthesis of pure phase NaP2 zeolite from the gel of NaY by conventional and microwave-assisted hydrothermal methods. *Crystals*, 10, 951.
- Viennet, J. C., Bultel, B., Riu, L., & Werner, S. C. (2017). Dioctahedral phyllosilicates versus zeolites and carbonates versus zeolites competitions as constraints to understanding early mars alteration conditions. *Journal of Geophysical Research: Planets*, 122, 2328–2343.
- Viennet, J. C., Bernard, S., Le Guillou, C., Jacquemot, P., Balan, E., Delbes, L., Rigaud, B., Georgelin, T., & Jaber, M. (2019). Experimental clues for detecting biosignatures on Mars. *Geochemical Perspectives Letters*, 12, 28–33.
- Viennet, J. C., Bernard, S., Le Guillou, C., Sautter, V., Schmitt-Kopplin, P., Beyssac, O., Pont, S., Zanda, B., Hewins, R., & Remusat, L. (2020). Tardi-magmatic precipitation of Martian Fe/Mg-rich clay minerals via igneous differentiation. *Geochemical Perspectives Letters*, 14, 47–52.
- Viennet, J. C., Bernard, S., Le Guillou, C., Sautter, V., Grégoire, B., Jambon, A., Pont, S., Beyssac, O., Zanda, B., Hewins, R., & Remusat, L. (2021). Martian magmatic clay minerals forming vesicles: perfect niches for emerging life? *Astrobiology*, 21, 605–612.
- Viennet, J. C., Le Guillou, C., Baron, F., Balan, E., Criouet, I., Delbes, L., Blanchenet, A., Laurent, B., Remusat, L., & Bernard, S. (2022). Experimental investigation of Fe-clay/organic interactions under asteroidal conditions. *Geochimica Et Cosmochimica Acta*, 318, 352–365.
- Viennet, J. C., Roskosz, M., Nakamura, T., Beck, P., Baptiste, B., Lavina, B., Alp, E., Hu, M. Y., Zhao, J., Gounelle, M., Brunetto, R., Yurimoto, H., Noguchi, T., Okazaki, R., Yabuta, H., Naraoka, H., Sakamoto, K., Tachibana, S., Yada, T., & Tsuda, Y. (2023). Interaction between clay minerals and organics in asteroid Ryugu. *Geochemical Perspectives Letters*, 25, 8–12.

- Waite, J. H., Glein, C. R., Perryman, R. S., Teolis, B. D., Magee, B. A., Miller, G., Grimes, J., Perry, M. E., Miller, K. E., Bouquet, A., Lunine, J. I., Brockwell, T., & Bolton, S. J. (2017). Cassini finds molecular hydrogen in the Enceladus plume: Evidence for hydrothermal processes. *Science*, *356*, 155–159.
- Yamada, H. (1994). Formation of smectite crystals at high pressures and temperatures. *Clays and Clay Minerals*, *42*, 674–678.
- Yamada, H. (1995). Cooling rate dependency of the formation of smectite crystals from a high-pressure and high-temperature hydrous melt. *Clays and Clay Minerals*, *43*, 693–696.
- Zhang, D., Zhou, C. H., Lin, C. X., Tong, D. S., & Yu, W. H. (2010). Synthesis of clay minerals. *Applied Clay Science*, *50*, 1–11.
- Zhang, C., Petit, S., He, H., Villiéras, F., Razaftianamaharavo, A., Baron, F., Tao, Q., & Zhu, J. (2020). Crystal growth of smectite: a study based on the change in crystal chemistry and morphology of saponites with synthesis time. *ACS Earth and Space Chemistry*, *4*, 14–23.
- Zhang, L., Fu, X., Wang, A., & Ling, Z. (2022). Crystallinity effects on the vibrational spectral features of saponite: Implications for characterizing variable crystalline phyllosilicates on Mars. *Icarus*, *379*, 114951.
- Zhou, C. H., & Keeling, J. (2013). Fundamental and applied research on clay minerals: from climate and environment to nanotechnology. *Applied Clay Science*, *74*, 3–9.
- Zviagina, B. B., McCarty, D. K., Srodonón, J., & Drits, V. A. (2004). Interpretation of infrared spectra of dioctahedral smectites in the region of OH-stretching vibrations. *Clays and Clay Minerals*, *52*, 399–410.

Springer Nature or its licensor (e.g. a society or other partner) holds exclusive rights to this article under a publishing agreement with the author(s) or other rightsholder(s); author self-archiving of the accepted manuscript version of this article is solely governed by the terms of such publishing agreement and applicable law.